A New Algorithm for Convex Biclustering and Its Extension to the Compositional Data

Binhuan Wang
Department of Population Health
New York University School of Medicine

Lanqiu Yao
Department of Population Health
New York University School of Medicine

Jiyuan Hu
Department of Population Health
New York University School of Medicine

Huilin Li
Department of Population Health
New York University School of Medicine

arXiv:2011.12182v1 [stat.ME] 24 Nov 2020

Abstract

Biclustering is a powerful data mining technique that allows simultaneously clustering rows (observations) and columns (features) in a matrix-format data set, which can provide results in a checkerboard-like pattern for visualization and exploratory analysis in a wide array of domains. Multiple biclustering algorithms have been developed in the past two decades, among which the convex biclustering can guarantee a global optimum by formulating in as a convex optimization problem. On the other hand, the application of biclustering has not progressed in parallel with the algorithm design. For example, biclustering for increasingly popular microbiome research data is under-applied, and one reason may be its compositional constraints. In this manuscript, we propose a new convex biclustering algorithm, called the bi-ADMM, under general setups based on the ADMM algorithm, which is free of extra smoothing steps to obtain informative biclusters required by existing convex biclustering algorithms. Furthermore, we tailor it to the algorithm named biC-ADMM specifically to tackle compositional constraints confronted in microbiome data. The key step of our methods utilizes the *Sylvester Equation*, which is new to the clustering research. The effectiveness of the proposed methods is examined through a variety of numerical experiments and a microbiome data application.

Key words: *Compositional data; Convex biclustering; Microbiome data; Sylvester Equation*

1 Introduction

Biclustering is a powerful data mining technique that allows simultaneously clustering rows (observations) and columns (features) in a matrix-format data set. It is a 2-way extension of clustering analysis which aims to assign observations into a number of clusters such that observations in

the same group are similar to each other. Biclustering can provide results in a checkerboard-like pattern, which can be used for visualization and exploratory analysis in a wide array of domains. For example, Cheng and Church (2000) introduced the concept of biclustering for the first time to gene expression data, aiming to overcome some problems of traditional clustering methods such as information lost during oversimplied similarity and grouping computation. Instead, biclustering identified co-expressed genes under a subset of all the conditions/samples, which provided a better representation for genes with multiple functions or regulated by many factors. Furthermore, in the big data era, electronic health record (EHR) contains abundant information that can be transformed into disease phenotypes. These phenotype data can be organized into a matrix, with individuals as rows and phenotype features as columns, from which biclustering can discover a subgroup of patients from a subset of phenotypes (Hripcsak and Albers, 2012). Results from biclustering can shed lights on the downstream analyses to interpret the identified biclusters and to demonstrate bicluster associations coupled with other statistical evaluations tool.

In the past two decades, multiple biclustering algorithms have been developed. The most popular approach for genomics data is the clustered dendrogram (Busygin et al., 2008; Madeira and Oliveira, 2004), which actually performs the hierarchical clustering (Friedman et al., 2001) on both subjects and genes. However, dendrogram is less ideal for generating reproducible results because it greedily fuses observations or features to minimize a specific objective function such as the within-clustering variance. As a consequence, this algorithm may return a locally optimal solution with respect to the criterion, and dendrogram is not stable to small perturbations of the data due to its greedy algorithm. Later on, more advanced biclustering methods have been proposed, which are either based on the singular value decomposition (SVD) or graph cuts. However, Chi et al. (2017) pointed out that none of these methods addressed the fundamental issues that underlay the clustered dendrogram. Alternatively, they formulated the biclustering problem as a convex optimization problem, and solved it with an iterative algorithm based on the splitting methods for convex clustering.

On the other hand, application of biclustering has not progressed in parallel with the algorithm

design. Recently, Xie et al. (2018) provided a comprehensive review of biclustering applications in biological and biomedical data, and pointed out there is a need for developing supporting computational techniques and providing the guidance on selecting the appropriate biclustering tools in a specific study. Data generated from different biotechnologies have their own properties. For example, 16S and shotgun sequencing are two widely used sequencing techniques in microbiome studies. The raw microbiome data are typically organized into large matrices with rows representing samples, and columns containing observed counts of clustered sequences commonly known as operational taxonomic units (OTUs). Due to the limitations of the sequencing techniques used in the microbiome research, the microbial profile usually is quantified in composition, i.e., a sum-to-one constraint. Because the observed counts are not comparable across samples due to their constrained total by the sequencing depth (Gloor et al., 2017), normalizing counts toward their totals into the relative abundance is a commonly used metric in microbiome studies, which imposes a compositional constraint for data from each sample. As reviewed by Xie et al. (2018), there are limited applications of biclustering in microbiome studies, except one example. Falony et al. (2016) identified sample subsets with specific taxonomic signatures using a biclustering approach called FABIA, proposed by Hochreiter et al. (2010).

In this manuscript, we propose a new convex biclustering algorithm bi-ADMM under general setups based on the alternating direction method of multipliers (ADMM) algorithm. Furthermore, we tailor it to the algorithm named biC-ADMM specifically to tackle the compositional constraints confronted in microbiome data. As far as we have known, it is the first biclustering algorithm that can handle data with compositional constraints. Compared with Chi et al. (2017), the novelty of this paper is two-fold. First, we solve the convex biclustering problem via the ADMM algorithm directly, while Chi et al. (2017) solved it by a convex bicluster ring algorithm (COBRA) via iteratively using Dykstra-like proximal algorithm (DLPA). Their methods require extra smoothing steps to obtain informative biclusters. The key step of our methods utilizes the *Sylvester Equation* for the first time to solve the challenging estimation problem involving both rows and columns of a matrix. Second, the proposed algorithms can naturally incorporate additional constraints for rows

or columns. For example, the modified algorithms for the microbiome data with compositional constraint for data rows are provided. Note that our methods are not only theoretical sound, but also practically promising. The superior performance of our methods is demonstrated in extensive simulated examples and the application to analyze a murine gut microbiome dataset (Livanos et al., 2016).

We demonstrate the superior performance of the proposed algorithm under the simulation setting in Section 4.1 with $\sigma = 4$, where σ is the standard deviation of the random noise for data generation. In this setting, there are $n = 80$ samples from 4 clusters and $p = 40$ features from 4 clusters. Figure 1 compares the performance of COBRA without the smoothing step (indicated as COBRA on the left panel) and our method (indicated as bi-ADMM on the right panel), by visualizing the estimate for each method with the same set of weights and the same value for the single tuning parameter, $\gamma = 6.72$. The heat maps show that the proposed bi-ADMM algorithm can directly output a clear checkerboard-like pattern without any further procedure.

Figure 1: The heat maps of estimated matrices based on the COBRA (left) and the bi-ADMM (right) algorithms with the same tuning parameter $\gamma = 6.72$, respectively. Rows indicate 80 samples with 4 clusters and columns indicate 40 features with 4 clusters. The row(column) side color bars indicate the true row(column) clusters.

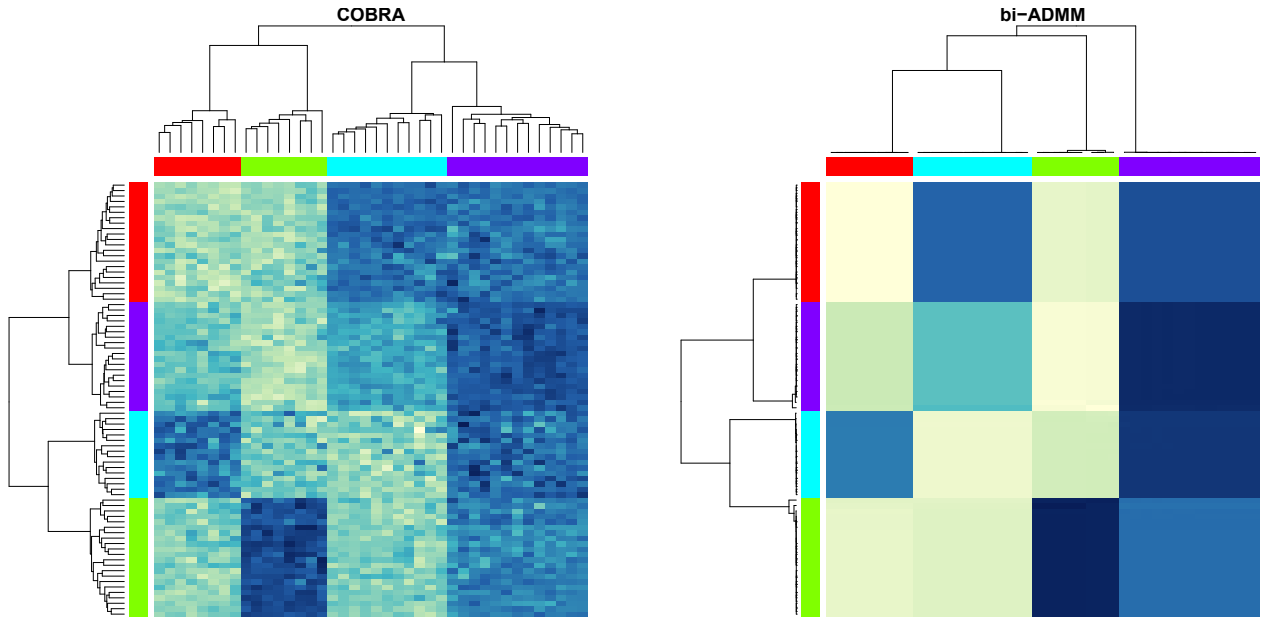

The rest of the paper is organized as follows. We propose the main methods and algorithms in Section 2. Some practical issues for applying the proposed algorithms are discussed in Section 3. The performance of the proposed methods via simulation studies are evaluated in Section 4, and a microbiome application is presented in Section 5. We conclude the paper with a brief summary in Section 6, and defer all technical proofs to the Appendix.

2 Convex Biclustering

This section presents the main results. We develop algorithms for a general biclustering problem first, and then extend them to incorporate the compositional constraints, a unique feature of the microbiome data.

2.1 Specification of the General Model

We consider a general biclustering problem as follows. Let $\mathbf{X} \in \mathbb{R}^{n\times p}$ be a data matrix with n observations $X_{i\cdot} = (X_{i1}, \ldots, X_{ip})^{\mathrm{T}}$ with p features, $i = 1, \cdots, n$. The underlying assumption for applying a biclustering method is that the n observations belong to K unknown and non-overlapping classes, $C_1, \ldots, C_K$, and the p features belong to R unknown and non-overlapping classes, $D_1, \ldots, D_R$. Such checker-board like structure of a data matrix motivates researchers to use the fused-lasso penalty (Tibshirani et al., 2005) to fuse rows and columns simultaneously.

To facilitate further derivations, we rewrite the data matrix $\mathbf{X}$ in feature-level as column vectors $\mathbf{x}_j$ so that $\mathbf{X} = (\mathbf{x}_1, \cdots, \mathbf{x}_p)$, where $\mathbf{x}_j = (X_{1j}, \cdots, X_{nj})^{\mathrm{T}}$, $j = 1, \ldots, p$. Similarly we denote $\mathbf{A}$ in the feature-level consisting of column vectors $\mathbf{A} = (\mathbf{a}_1, \cdots, \mathbf{a}_p)$, where $\mathbf{a}_j = (A_{1j}, \cdots, A_{nj})^{\mathrm{T}}$, and as $(A_{1\cdot}, \ldots, A_{n\cdot})^{\mathrm{T}}$ in the observation-level. Define $\mathcal{E}_1 = \{l = (l_1, l_2) : 1 \leqslant l_1 < l_2 \leqslant n\}$ and $\mathcal{E}_2 = \{k = (k_1, k_2) : 0 \leqslant k_1 < k_2 \leqslant p\}$. Then denote $|\mathcal{E}_1|$ and $|\mathcal{E}_2|$ as the numbers of components of $\mathcal{E}_1$ and $\mathcal{E}_2$, respectively.

We formulate the convex biclustering problem as the following minimization problem with

tuning parameters γ_1 and γ_2:

$$\min_{\mathbf{A}\in\mathbb{R}^{p\times n}} \quad \frac{1}{2}\sum_{i=1}^{n}\|X_{i\cdot}-A_{i\cdot}\|_2^2+\gamma_1\sum_{l\in\mathcal{E}_1}w_l\|A_{l_1\cdot}-A_{l_2\cdot}\|_q+\gamma_2\sum_{k\in\mathcal{E}_2}u_k\|\mathbf{a}_{k_1}-\mathbf{a}_{k_2}\|_q, \tag{1}$$

where the weights $w_l \geqslant 0$ and $u_k \geqslant 0$. Wang et al. (2018) suggested $w_l = \iota_{l_1,l_2}^{m_1}\exp(-\phi\|X_{l_1\cdot}-X_{l_2\cdot}\|_2^2)$, where $\iota_{l_1,l_2}^{m_1}$ is 1 if observation l_2 is among l_1's m_1 nearest neighbors or vice verse, and 0 otherwise. Similarly, we suggest using $u_k = \iota_{k_1,k_2}^{m_2}\exp(-\phi\|\mathbf{x}_{k_1}-\mathbf{x}_{k_2}\|_2^2)$.

By incorporating the fused-lasso penalty in the second and third terms of (1), the above formulation encourages that some of the rows or columns of the solution $\widehat{\mathbf{A}}$ are identical. If $\widehat{A}_{l_1\cdot}=\widehat{A}_{l_2\cdot}$, then observation l_1 and observation l_2 will be assigned to the same observation (row) cluster; if $\widehat{\mathbf{a}}_{k_1}=\widehat{\mathbf{a}}_{k_2}$, then feature k_1 and feature k_2 will be assigned to the same feature (column) cluster. The tuning parameter γ_1 in (1) controls the number of unique rows of $\widehat{\mathbf{A}}$, that is, the number of estimated observation clusters, while the tuning parameter γ_2 controls the number of estimated feature clusters. When $\gamma_1=\gamma_2=0$, $\widehat{\mathbf{A}}=\mathbf{X}$, and thus, each combination of feature and observation by itself is a bicluster. As γ_1 and γ_2 increases, some of the rows and columns of $\widehat{\mathbf{A}}$ become identical, respectively, which demonstrates a fusing process. For sufficiently large γ_1 and γ_2, all rows or columns of $\widehat{\mathbf{A}}$ will be identical, implying that all observations or features are estimated to form a single bicluster. With such a strictly convex objective function in (1), the solution $\widehat{\mathbf{A}}$ from convex biclustering is unique for each given pair of γ_1 and γ_2.

2.2 bi-ADMM: a Biclustering Algorithm for the General Model

In order to implement the ADMM algorithm, we rewrite the above problem into the following constrained optimization problem:

$$\begin{aligned}\min_{\mathbf{A}\in\mathbb{R}^{p\times n}} \quad & \frac{1}{2}\sum_{i=1}^{n}\|X_{i\cdot}-A_{i\cdot}\|_2^2+\gamma_1\sum_{l\in\mathcal{E}_1}w_l\|\mathbf{v}_l\|_q+\gamma_2\sum_{k\in\mathcal{E}_2}u_k\|\mathbf{z}_k\|_q \\ \text{s.t.} \quad & A_{l_1\cdot}-A_{l_2\cdot}-\mathbf{v}_l=\mathbf{0},\ \forall l\in\mathcal{E}_1 \\ & \mathbf{a}_{k_1}-\mathbf{a}_{k_2}-\mathbf{z}_k=\mathbf{0},\ \forall k\in\mathcal{E}_2,\end{aligned} \tag{2}$$

which is also equivalent to an augmented Lagrangian problem given by

$$\begin{aligned}\mathcal{L}_{\nu_1,\nu_2}(\mathbf{A},\mathbf{V},\mathbf{Z},\mathbf{\Lambda}_1,\mathbf{\Lambda}_2) &= \frac{1}{2}\sum_{i=1}^{n}\|X_{i\cdot}-A_{i\cdot}\|_2^2+\gamma_1\sum_{l\in\mathcal{E}_1}w_l\|\mathbf{v}_l\|_q+\gamma_2\sum_{k\in\mathcal{E}_2}u_k\|\mathbf{z}_k\|_q \\ &\quad+\sum_{l\in\mathcal{E}_1}\langle\boldsymbol{\lambda}_{1l},\mathbf{v}_l-A_{l_1\cdot}+A_{l_2\cdot}\rangle+\frac{\nu_1}{2}\sum_{l\in\mathcal{E}_1}\|\mathbf{v}_l-A_{l_1\cdot}+A_{l_2\cdot}\|_2^2 \\ &\quad+\sum_{k\in\mathcal{E}_2}\langle\boldsymbol{\lambda}_{2k},\mathbf{z}_k-\mathbf{a}_{k_1}+\mathbf{a}_{k_2}\rangle+\frac{\nu_2}{2}\sum_{k\in\mathcal{E}_2}\|\mathbf{z}_k-\mathbf{a}_{k_1}+\mathbf{a}_{k_2}\|_2^2, \quad (3)\end{aligned}$$

where ν_1 and ν_2 are nonnegative constants, $\mathbf{V}=(\mathbf{v}_1,\ldots,\mathbf{v}_{|\mathcal{E}_1|})$, $\mathbf{Z}=(\mathbf{z}_1,\ldots,\mathbf{z}_{|\mathcal{E}_2|})$, $\mathbf{\Lambda}_1=(\boldsymbol{\lambda}_{11},\ldots,\boldsymbol{\lambda}_{1|\mathcal{E}_1|})$ and $\mathbf{\Lambda}_2=(\boldsymbol{\lambda}_{21},\ldots,\boldsymbol{\lambda}_{2|\mathcal{E}_2|})$. This optimization problem is challenging in dealing with fusing both observation-level and feature-level vectors in the objective function simultaneously.

The bi-ADMM minimizes the augmented Lagrangian problem by alternatively solving one block of variables at a time. Specifically, bi-ADMM solves

$$\begin{aligned}\mathbf{A}^{m+1} &= \operatorname*{argmin}_{\mathbf{A}}\mathcal{L}_{\nu_1,\nu_2}(\mathbf{A},\mathbf{V}^m,\mathbf{Z}^m,\mathbf{\Lambda}_1^m,\mathbf{\Lambda}_2^m), \\ \mathbf{V}^{m+1} &= \operatorname*{argmin}_{\mathbf{V}}\mathcal{L}_{\nu_1,\nu_2}(\mathbf{A}^{m+1},\mathbf{V},\mathbf{Z}^m,\mathbf{\Lambda}_1^m,\mathbf{\Lambda}_2^m), \\ \mathbf{Z}^{m+1} &= \operatorname*{argmin}_{\mathbf{Z}}\mathcal{L}_{\nu_1,\nu_2}(\mathbf{A}^{m+1},\mathbf{V}^{m+1},\mathbf{Z},\mathbf{\Lambda}_1^m,\mathbf{\Lambda}_2^m), \quad (4) \\ \boldsymbol{\lambda}_{1l}^{m+1} &= \boldsymbol{\lambda}_{1l}^m+\nu_1(\mathbf{v}_l^{m+1}-A_{l_1\cdot}^{m+1}+A_{l_2\cdot}^{m+1}),\ l\in\mathcal{E}_1, \\ \boldsymbol{\lambda}_{2k}^{m+1} &= \boldsymbol{\lambda}_{2k}^m+\nu_2(\mathbf{z}_k^{m+1}-\mathbf{a}_{k_1}^{m+1}+\mathbf{a}_{k_2}^{m+1}),\ k\in\mathcal{E}_2.\end{aligned}$$

Next, we develop the detailed updating implementations for $\mathbf{A},\mathbf{V},\mathbf{Z},\mathbf{\Lambda}_1$ and $\mathbf{\Lambda}_2$ in three steps. A summary of the bi-ADMM algorithm is shown in Algorithm 1.

Step 1: update $\mathbf{A}$. To update $\mathbf{A}$, we need to minimize

$$f(\mathbf{A}) = \frac{1}{2}\sum_{i=1}^{n}\|X_{i\cdot}-A_{i\cdot}\|_2^2+\frac{\nu_1}{2}\sum_{l\in\mathcal{E}_1}\|\widetilde{\mathbf{v}}_l-A_{l_1\cdot}+A_{l_2\cdot}\|_2^2+\frac{\nu_2}{2}\sum_{k\in\mathcal{E}_2}\|\widetilde{\mathbf{z}}_k-\mathbf{a}_{k_1}+\mathbf{a}_{k_2}\|_2^2, \quad (5)$$

where $\widetilde{\mathbf{v}}_1=\mathbf{v}_l+\frac{1}{\nu_1}\boldsymbol{\lambda}_{1l}$ and $\widetilde{\mathbf{z}}_k=\mathbf{z}_k+\frac{1}{\nu_2}\boldsymbol{\lambda}_{2k}$.

The optimization problem is challenging because it involves both rows and columns of a single

matrix. To tackle this difficulty, the following key lemma associating (5) with a *Sylvester Equations* is proposed. The proof of Lemma 1 is provided in Appendix.

Lemma 1 *Let $\mathbf{I}_n$ be an $n \times n$ identity matrix, $\mathbf{1}_n$ be an n-dimensional vector with each component being 1, $\mathbf{e}_i$ be an n-dimensional vector with all components being 0, except the i-th component being 1, and $\mathbf{e}_j^*$ is a p-dimensional vector with the j-th element as 1 and 0 otherwise. In addition, define*

$$\begin{aligned}
\mathbf{M} &= \mathbf{I}_n + \nu_1 \sum_{l \in \mathcal{E}_1} (\mathbf{e}_{l_1} - \mathbf{e}_{l_2})(\mathbf{e}_{l_1} - \mathbf{e}_{l_2})^{\mathrm{T}} \\
\mathbf{N} &= \nu_2 \sum_{k \in \mathcal{E}_2} (\mathbf{e}_{k_1}^* - \mathbf{e}_{k_2}^*)(\mathbf{e}_{k_1}^* - \mathbf{e}_{k_2}^*)^{\mathrm{T}} \\
\mathbf{G} &= \mathbf{X} + \sum_{l \in \mathcal{E}_1} (\mathbf{e}_{l_1} - \mathbf{e}_{l_2})(\boldsymbol{\lambda}_{1l} + \nu_1 \mathbf{v}_l)^{\mathrm{T}} + \sum_{k \in \mathcal{E}_2} (\boldsymbol{\lambda}_{2k} + \nu_2 \mathbf{z}_k)(\mathbf{e}_{k_1}^* - \mathbf{e}_{k_2}^*)^{\mathrm{T}}.
\end{aligned}$$

Then, minimizing (5) is equivalent to solving the following Sylvester Equation

$$\mathbf{MA} + \mathbf{AN} = \mathbf{G}. \tag{6}$$

If the edge sets $\mathcal{E}_1$ and $\mathcal{E}_2$ contain all possible edges, it is straightforward to verify

$$\begin{aligned}
\sum_{l \in \mathcal{E}_1} (\mathbf{e}_{l_1} - \mathbf{e}_{l_2})(\mathbf{e}_{l_1} - \mathbf{e}_{l_2})^{\mathrm{T}} &= n\mathbf{I}_n - \mathbf{1}_n \mathbf{1}_n^{\mathrm{T}} \\
\sum_{k \in \mathcal{E}_2} (\mathbf{e}_{k_1}^* - \mathbf{e}_{k_2}^*)(\mathbf{e}_{k_1}^* - \mathbf{e}_{k_2}^*)^{\mathrm{T}} &= p\mathbf{I}_p - \mathbf{1}_p \mathbf{1}_p^{\mathrm{T}}.
\end{aligned}$$

Then, $\mathbf{M} = (1 + n\nu_1)\mathbf{I}_n - \nu_1 \mathbf{1}_n \mathbf{1}_n^{\mathrm{T}}$ and $\mathbf{N} = p\nu_2 \mathbf{I}_p - \nu_2 \mathbf{1}_p \mathbf{1}_p^{\mathrm{T}}$.

The type of equation (6) is called *Sylvester Equation*, which is very important in control theory and many other branches of engineering. Its theoretical solution is based on eigenvector and eigenvalue decomposition (Jameson, 1968), but it is computationally expensive. Alternatively, we implement an efficient algorithm to solve it, proposed by Sorensen et al. (2003).

Step 2: Update V and Z. For any $\sigma > 0$ and norm $\Omega(\cdot)$, we define a proximal map,

$$\text{prox}_{\sigma\Omega}(\mathbf{u}) = \underset{\mathbf{v}}{\text{argmin}} \left[\sigma\Omega(\mathbf{v}) + \frac{1}{2}\|\mathbf{u} - \mathbf{v}\|_2^2 \right].$$

We refer the readers to Table 1 in Chi and Lange (2015) for the explicit formulations of the proximal map of q-norm for $q = 1, 2$ and ∞. It is clear that the vectors $\mathbf{v}_l$ and $\mathbf{z}_k$ are separable in the objective function (3), and thus $\mathbf{v}_l$ and $\mathbf{z}_k$ can be solved via proximal maps:

$$\begin{aligned}
\mathbf{v}_l &= \underset{\mathbf{v}_l}{\text{argmin}} \frac{1}{2}\|\mathbf{v}_l - (A_{l_1\cdot} - A_{l_2\cdot} - \nu_1^{-1}\boldsymbol{\lambda}_{1l})\|_2^2 + \frac{\gamma_1 w_l}{\nu_1}\|\mathbf{v}_l\|_q \\
&= \text{prox}_{\sigma_{1l}\|\cdot\|_q}(A_{l_1\cdot} - A_{l_2\cdot} - \nu_1^{-1}\boldsymbol{\lambda}_{1l}) \\
\mathbf{z}_k &= \underset{\mathbf{z}_k}{\text{argmin}} \frac{1}{2}\|\mathbf{z}_k - (\mathbf{a}_{k_1} - \mathbf{a}_{k_2} - \nu_2^{-1}\boldsymbol{\lambda}_{2k})\|_2^2 + \frac{\gamma_2 u_k}{\nu_2}\|\mathbf{z}_k\|_q \\
&= \text{prox}_{\sigma_{2k}\|\cdot\|_q}(\mathbf{a}_{k_1} - \mathbf{a}_{k_2} - \nu_2^{-1}\boldsymbol{\lambda}_{2k}),
\end{aligned}$$

where $\sigma_{1l} = \gamma_1 w_l/\nu_1$ and $\sigma_{2k} = \gamma_2 u_k/\nu_2$.

Step 3: Update $\boldsymbol{\Lambda}_1$ and $\boldsymbol{\Lambda}_2$. Finally, $\boldsymbol{\lambda}_{1l}$ and $\boldsymbol{\lambda}_{2k}$ can be updated by $\boldsymbol{\lambda}_{1l} = \boldsymbol{\lambda}_{1l} + \nu_1(\mathbf{v}_l - A_{l_1\cdot} + A_{l_2\cdot})$ and $\boldsymbol{\lambda}_{2k} = \boldsymbol{\lambda}_{2k} + \nu_2(\mathbf{z}_k - \mathbf{a}_{k_1} + \mathbf{a}_{k_2})$.

2.3 biC-ADMM: Biclustering Algorithm for Model with Compositional Constraints

For microbiome data, due to its data-generating mechanism, the counts of all taxa need to be normalized into the relative abundances such that their summation for each sample is 1. This type of data is also called compositional data in mathematics. Our newly proposed clustering algorithm, biC-ADMM, aims to incorporate the compositional constraint into the optimization. To be specific, the data from each sample satisfy $X_{i\cdot}^{\mathrm{T}}\mathbf{1}_p = 1, i = 1, \ldots, n$, and then it is natural to require the estimate $\mathbf{A}$ to satisfy the same constraints, i.e., $A_{i\cdot}^{\mathrm{T}}\mathbf{1}_p = 1$.

Because the bi-ADMM solves an optimization problem with constraints, it can be easily extended to the biC-ADMM algorithm by incorporating the compositional constraints. With the ad-

Algorithm 1 bi-ADMM

1. Initialize $\mathbf{V}^0, \mathbf{Z}^0, \mathbf{\Lambda}_1^0$ and $\mathbf{\Lambda}_2^0$. Calculate

$$\begin{aligned}\mathbf{M} &= \mathbf{I}_n + \nu_1 \sum_{l\in\mathcal{E}_1}(\mathbf{e}_{l_1} - \mathbf{e}_{l_2})(\mathbf{e}_{l_1} - \mathbf{e}_{l_2})^{\mathrm{T}} \\ \mathbf{N} &= \nu_2 \sum_{k\in\mathcal{E}_2}(\mathbf{e}^*_{k_1} - \mathbf{e}^*_{k_2})(\mathbf{e}^*_{k_1} - \mathbf{e}^*_{k_2})^{\mathrm{T}}\end{aligned}$$

   For $m = 1, 2, \ldots$

2. Solve the Sylvester equation $\mathbf{MA} + \mathbf{AN} = \mathbf{G}^{m-1}$ to obtain $\mathbf{A}^m$, where

$$\mathbf{G}^{m-1} = \mathbf{X} + \sum_{l\in\mathcal{E}_1}(\mathbf{e}_{l_1} - \mathbf{e}_{l_2})(\boldsymbol{\lambda}_{1l}^{m-1} + \nu_1\mathbf{v}_l^{m-1})^{\mathrm{T}} + \sum_{k\in\mathcal{E}_2}(\boldsymbol{\lambda}_{2k}^{m-1} + \nu_2\mathbf{z}_k^{m-1})(\mathbf{e}^*_{k_1} - \mathbf{e}^*_{k_2})^{\mathrm{T}}.$$

3. For $l \in \mathcal{E}_1$, do

$$\mathbf{v}_l^m = \mathrm{prox}_{\sigma_{1l}\|\cdot\|_q}(A^m_{l_1\cdot} - A^m_{l_2\cdot} - \nu_1^{-1}\boldsymbol{\lambda}_{1l}^{m-1}).$$

4. For $k \in \mathcal{E}_2$, do

$$\mathbf{z}_l^m = \mathrm{prox}_{\sigma_{2k}\|\cdot\|_q}(\mathbf{a}^m_{k_1} - \mathbf{a}^m_{k_2} - \nu_2^{-1}\boldsymbol{\lambda}_{2k}^{m-1}).$$

5. For $l \in \mathcal{E}_1$ and $k \in \mathcal{E}_2$, do

$$\begin{aligned}\boldsymbol{\lambda}_{1l}^m &= \boldsymbol{\lambda}_{1l}^{m-1} + \nu_1(\mathbf{v}_l^m - A^m_{l_1\cdot} + A^m_{l_2\cdot}) \\ \boldsymbol{\lambda}_{2k}^m &= \boldsymbol{\lambda}_{2k}^{m-1} + \nu_2(\mathbf{z}_k^m - \mathbf{a}^m_{k_1} + \mathbf{a}^m_{k_2})\end{aligned}$$

6. Repeat Steps 2-5 until convergence.

ditional compositional constraints into (2), the augmented Lagrangian problem for compositional data is given by

$$\begin{aligned}\mathcal{L}_{\nu_1,\nu_2,\nu_3}(\mathbf{A}, \mathbf{V}, \mathbf{Z}, \mathbf{\Lambda}_1, \mathbf{\Lambda}_2, \boldsymbol{\lambda}_3) &= \frac{1}{2}\sum_{i=1}^n \|X_{i\cdot} - A_{i\cdot}\|_2^2 + \gamma_1 \sum_{l\in\mathcal{E}_1} w_l\|\mathbf{v}_l\|_q + \gamma_2 \sum_{k\in\mathcal{E}_2} u_k\|\mathbf{z}_k\|_q \\ &+ \sum_{l\in\mathcal{E}_1}\langle\boldsymbol{\lambda}_{1l}, \mathbf{v}_l - A_{l_1\cdot} + A_{l_2\cdot}\rangle + \frac{\nu_1}{2}\sum_{l\in\mathcal{E}_1}\|\mathbf{v}_l - A_{l_1\cdot} + A_{l_2\cdot}\|_2^2 \\ &+ \sum_{k\in\mathcal{E}_2}\langle\boldsymbol{\lambda}_{2k}, \mathbf{z}_k - \mathbf{a}_{k_1} + \mathbf{a}_{k_2}\rangle + \frac{\nu_2}{2}\sum_{k\in\mathcal{E}_2}\|\mathbf{z}_k - \mathbf{a}_{k_1} + \mathbf{a}_{k_2}\|_2^2 \\ &+ \langle\boldsymbol{\lambda}_3, \mathbf{1}_n - \mathbf{A}\mathbf{1}_p\rangle + \frac{\nu_3}{2}\|\mathbf{1}_n - \mathbf{A}\mathbf{1}_p\|_2^2, \qquad (7)\end{aligned}$$

where ν_3 is a nonnegative constant and $\boldsymbol{\lambda}_3 = (\lambda_{31}, \ldots, \lambda_{3n})^{\mathrm{T}}$.

As a variant of the bi-ADMM for biclustering compositional data, the biC-ADMM algorithm is similar with the bi-ADMM detailed in Section 2.2. The key step for updating $\mathbf{A}$ of the biC-ADMM is summarized in the following Lemma 2, which minimizes:

$$f(\mathbf{a}) = \frac{1}{2}\|\mathbf{x} - \mathbf{a}\|_2^2 + \frac{\nu_1}{2}\|\mathbf{B}\mathbf{P}\mathbf{a} - \widetilde{\mathbf{v}}\|_2^2 + \frac{\nu_2}{2}\|\mathbf{C}\mathbf{a} - \widetilde{\mathbf{z}}\|_2^2 + \frac{\nu_3}{2}\|\mathbf{D}\mathbf{a} - \mathbf{s}\|_2^2, \tag{8}$$

with $\mathbf{x} = \mathrm{vec}(\mathbf{X})$, $\mathbf{a} = \mathrm{vec}(\mathbf{A})$, the vectorization of the matrices $\mathbf{X}$ and $\mathbf{A}$, and

$$\begin{aligned}
\mathbf{B}^{\mathrm{T}} &= \left(\mathbf{B}_1^{\mathrm{T}}, \ldots, \mathbf{B}_{|\mathcal{E}_1|}^{\mathrm{T}}\right), \quad \widetilde{\mathbf{v}}^{\mathrm{T}} = \left(\widetilde{\mathbf{v}}_1^{\mathrm{T}}, \ldots, \widetilde{\mathbf{v}}_{|\mathcal{E}_1|}^{\mathrm{T}}\right), \\
\mathbf{C}^{\mathrm{T}} &= \left(\mathbf{C}_1^{\mathrm{T}}, \ldots, \mathbf{C}_{|\mathcal{E}_2|}^{\mathrm{T}}\right), \quad \widetilde{\mathbf{z}}^{\mathrm{T}} = \left(\widetilde{\mathbf{z}}_1^{\mathrm{T}}, \ldots, \widetilde{\mathbf{z}}_{|\mathcal{E}_2|}^{\mathrm{T}}\right), \\
\mathbf{D}^{\mathrm{T}} &= \left(\mathbf{D}_1^{\mathrm{T}}, \ldots, \mathbf{D}_n^{\mathrm{T}}\right), \quad \mathbf{s} = (s_1, \ldots, s_n)^{\mathrm{T}} = \mathbf{1}_n + \boldsymbol{\lambda}_3/\nu_3,
\end{aligned}$$

where $\mathbf{B}_l = (\mathbf{e}_{l_1} - \mathbf{e}_{l2})^{\mathrm{T}} \otimes \mathbf{I}_p, \mathbf{C}_k = (\mathbf{e}_{k_1}^* - \mathbf{e}_{k2}^*)^{\mathrm{T}} \otimes \mathbf{I}_n, \mathbf{D}_i = \mathbf{1}_p^{\mathrm{T}} \otimes \mathbf{e}_i^{\mathrm{T}}$, and $\mathbf{P}$ is a permutation matrix such that $\mathrm{vec}(\mathbf{A}^{\mathrm{T}}) = \mathbf{P}\mathrm{vec}(\mathbf{A}), l = 1, \ldots, |\mathcal{E}_1|, k = 1, \ldots, |\mathcal{E}_2|, i = 1, \ldots, n$, respectively.

Lemma 2 *Define*

$$\begin{aligned}
\mathbf{M} &= \mathbf{I}_n + \nu_1 \sum_{l \in \mathcal{E}_1} (\mathbf{e}_{l_1} - \mathbf{e}_{l_2})(\mathbf{e}_{l_1} - \mathbf{e}_{l_2})^{\mathrm{T}} \\
\mathbf{N} &= \nu_2 \sum_{k \in \mathcal{E}_2} (\mathbf{e}_{k_1}^* - \mathbf{e}_{k_2}^*)(\mathbf{e}_{k_1}^* - \mathbf{e}_{k_2}^*)^{\mathrm{T}} + \nu_3 \mathbf{1}_p \mathbf{1}_p^{\mathrm{T}} \\
\mathbf{G} &= \mathbf{X} + \sum_{l \in \mathcal{E}_1} (\mathbf{e}_{l_1} - \mathbf{e}_{l_2})(\boldsymbol{\lambda}_{1l} + \nu_1 \mathbf{v}_l)^{\mathrm{T}} + \sum_{k \in \mathcal{E}_2} (\boldsymbol{\lambda}_{2k} + \nu_2 \mathbf{z}_k)(\mathbf{e}_{k_1}^* - \mathbf{e}_{k_2}^*)^{\mathrm{T}} + \nu_3 \mathbf{s} \mathbf{1}_p^{\mathrm{T}}.
\end{aligned}$$

Then, minimizing (8) *is equivalent to solving the following Sylvester Equation*

$$\mathbf{M}\mathbf{A} + \mathbf{A}\mathbf{N} = \mathbf{G}. \tag{9}$$

Proof of Lemma 2 is provided in the Appendix, and the biC-ADMM algorithm is summarized in Algorithm 2.

Algorithm 2 biC-ADMM

1. Initialize $\mathbf{V}^0, \mathbf{Z}^0, \mathbf{\Lambda}_1^0, \mathbf{\Lambda}_2^0$ and $\boldsymbol{\lambda}_3^0$. Calculate

$$\begin{aligned}\mathbf{M} &= \mathbf{I}_n + \nu_1 \sum_{l\in\mathcal{E}_1} (\mathbf{e}_{l_1} - \mathbf{e}_{l_2})(\mathbf{e}_{l_1} - \mathbf{e}_{l_2})^{\mathrm{T}} \\ \mathbf{N} &= \nu_2 \sum_{k\in\mathcal{E}_2} (\mathbf{e}_{k_1}^* - \mathbf{e}_{k_2}^*)(\mathbf{e}_{k_1}^* - \mathbf{e}_{k_2}^*)^{\mathrm{T}} + \nu_3 \mathbf{1}_p \mathbf{1}_p^{\mathrm{T}}\end{aligned}$$

   For $m = 1, 2, \ldots$

2. Solve the Sylvester equation $\mathbf{MA} + \mathbf{AN} = \mathbf{G}^{m-1}$ to obtain $\mathbf{A}^m$, where

$$\mathbf{G}^{m-1} = \mathbf{X} + \sum_{l\in\mathcal{E}_1} (\mathbf{e}_{l_1} - \mathbf{e}_{l_2})(\boldsymbol{\lambda}_{1l}^{m-1} + \nu_1 \mathbf{v}_l^{m-1})^{\mathrm{T}} + \sum_{k\in\mathcal{E}_2} (\boldsymbol{\lambda}_{2k}^{m-1} + \nu_2 \mathbf{z}_k^{m-1})(\mathbf{e}_{k_1}^* - \mathbf{e}_{k_2}^*)^{\mathrm{T}} + \nu_3 \mathbf{s}^{m-1} \mathbf{1}_p^{\mathrm{T}},$$

   where $\mathbf{s}^{m-1} = \mathbf{1}_n + \boldsymbol{\lambda}_3^{m-1}/\nu_3$.

3. For $l \in \mathcal{E}_1$, do

$$\mathbf{v}_l^m = \mathrm{prox}_{\sigma_{1l}\|\cdot\|_q}(A_{l_1\cdot}^m - A_{l_2\cdot}^m - \nu_1^{-1}\boldsymbol{\lambda}_{1l}^{m-1}).$$

4. For $k \in \mathcal{E}_2$, do

$$\mathbf{z}_l^m = \mathrm{prox}_{\sigma_{2k}\|\cdot\|_q}(\mathbf{a}_{k_1}^m - \mathbf{a}_{k_2}^m - \nu_2^{-1}\boldsymbol{\lambda}_{2k}^{m-1}).$$

5. For $l \in \mathcal{E}_1$ and $k \in \mathcal{E}_2$, do

$$\begin{aligned}\boldsymbol{\lambda}_{1l}^m &= \boldsymbol{\lambda}_{1l}^{m-1} + \nu_1(\mathbf{v}_l^m - A_{l_1\cdot}^m + A_{l_2\cdot}^m) \\ \boldsymbol{\lambda}_{2k}^m &= \boldsymbol{\lambda}_{2k}^{m-1} + \nu_2(\mathbf{z}_k^m - \mathbf{a}_{k_1}^m + \mathbf{a}_{k_2}^m) \\ \boldsymbol{\lambda}_3^m &= \boldsymbol{\lambda}_3^{m-1} + \nu_3(\mathbf{1}_n - \mathbf{A}^m \mathbf{1}_p)\end{aligned}$$

6. Repeat Steps 2-5 until convergence.

3 Implementation of bi-ADMM and biC-ADMM in Practical Settings

In this section, we discuss a few practical issues for implementing the proposed algorithms, including algorithmic convergence and selection of tuning parameters. The weights w_l and u_k are suggested in Section 2.1.

3.1 Algorithmic Convergence

The proposed convex biclustering algorithms are derived by applying standard techniques of the ADMM method. For convex clustering problems, Chi and Lange (2015) and Wang et al. (2018)

as well as the references therein provided sufficient conditions for the convergence of their proposed methods. Chi et al. (2017) discussed the convergence of their algorithm COBRA for convex biclustering problem.

The convergence of our bi-ADMM and biC-ADMM algorithms follows similar arguments. Note that the only difference between the objective function in (1) and its counterpart in Chi and Lange (2015) is an additional fused-lasso penalty term for feature-level vectors, which is strongly convex. According to Chi and Lange (2015), one can show that, under mild regularization conditions, the convergence of the bi-ADMM and biC-ADMM algrithms is guaranteed for any $\nu_j > 0, j = 1, 2, 3$.

3.2 Selection of Tuning Parameters

This subsection discusses the methods for selecting tuning parameters γ_1 and γ_2. Recall that γ_1 controls the number of estimated observation-level clusters and γ_2 controls the number of estimated feature-level clusters.

Generally speaking, a two-dimensional grid search can provide an optimal pair of tuning parameters under some criterion if the computational resource is powerful enough. If the data matrix is in a large scale, we may adopt a similar strategy suggested in Chi et al. (2017) by using a single tuning parameter γ for properly rescaled penalty terms. To be specific, we rewrite the convex biclustering problem as the following minimization problem with a single tuning parameter γ:

$$\min_{\mathbf{A}\in\mathbb{R}^{p\times n}} \quad \frac{1}{2}\sum_{i=1}^{n}\|X_{i\cdot} - A_{i\cdot}\|_2^2 + \gamma\left\{\sum_{l\in\mathcal{E}_1} w_l\|A_{l_1\cdot} - A_{l_2\cdot}\|_q + \sum_{k\in\mathcal{E}_2} u_k\|\mathbf{a}_{k_1} - \mathbf{a}_{k_2}\|_q\right\}. \tag{10}$$

The key to the validity of this formulation is that the two penalty terms $\sum_{l\in\mathcal{E}_1} w_l\|A_{l_1\cdot} - A_{l_2\cdot}\|_q$ and $\sum_{k\in\mathcal{E}_2} u_k\|\mathbf{a}_{k_1} - \mathbf{a}_{k_2}\|_q$ should be on the same scale. Note that row vectors of $\mathbf{A}$ are in $\mathbb{R}^p$ while column vectors of $\mathbf{A}$ are in $\mathbb{R}^n$. Thus, we choose row weights w_l to sum to $1/\sqrt{p}$ and the column weights u_k to sum to $1/\sqrt{n}$.

Next, we discuss two criteria for tuning parameter selection in a data-driven manner. One is

spiritually similar with cross-validation and the other is based on stability selection. Chi et al. (2017) proposed a hold-out validation method for convex biclustering by randomly selecting a hold-out of elements in the data matrix and assessing the quality of predicting the hold-out set with an estimated model based on the rest elements. Alternatively, Wang et al. (2018) proposed to use stability selection in Fang and Wang (2012) to tune two parameters for sparse convex clustering. For convex biclustering, we can apply stability section in a similar way to tune γ_1 and γ_2. To be specific, for any given γ_1 and γ_2, two biclustering results can be produced via (1) based on two sets of bootstrapped samples, and then the stability measurement (Fang and Wang, 2012) can be computed to measure the agreement between the two biclustering results. A repetition of this procedure for 50 times is required to enhance the robustness of the stability selection method. Finally, the optimal parameters are selected as the one achieving maximum averaged stability value.

4 Simulation Studies

In this section, we conduct simulation studies to thoroughly evaluate the performance of the proposed bi-ADMM under general biclustering setups and the biC-ADMM under scenarios with compositional constrains motivated by a real microbiome dataset Livanos et al. (2016), and compare them with the competing method COBRA. For each setting, we run 100 repetitions. In all simulation studies, the adjusted-RAND index (ARI) (Hubert and Arabie, 1985) is used to measure the agreement between the estimated clustering result and the underlying true clustering assignment. The ARI ranges from 0 to 1 with a higher value indicating better performance. Note that the underlying cluster labels are known or pre-specified in simulation studies, and thus, it is feasible to evaluate how well the candidate methods can perform if they are tuned by maximizing the ARI. To ensure fair comparisons, for each repetition, a separate validation sample is generated to select an optimal tuning parameter γ for both algorithm under the formulation shown in (10), which involves a single tuning parameter. For each repetition, The best tuning parameter is chosen by maximizing

the ARI on the validation data set.

4.1 General Setups

To generate datasets with checkerboard cluster structures, we consider various sizes of datasets with n observations (row) and p features (column), where (n, p) are set as $(50, 40), (100, 80), (200, 160)$, respectively. The number of row and column clusters varies as well. Given the dataset size, $K = 4, 8, 12$, or 16 row clusters and $R = 4, 8$, or 16 column clusters are generated accordingly. The corresponding total number of biclusters are $M \doteq K \times R = 16, 32, 64, 96, 128$, or 256.

X_{ij} is generated as follows. First, we assign cluster indexes to the observations (rows) by sampling from a set $\{1, ..., K\}$ uniformly, and the cluster indexes are assigned to features (columns) following a similar procedure. Thus, each X_{ij} belongs to one of those M biclusters. Second, random samples for each bicluster are generated from a normal distribution, X_{ij} i.i.d. $\sim \mathcal{N}(\mu_{kr}, \sigma^2)$, i.e., samples from the row cluster $k \in \{1, \ldots, K\}$ and column cluster $r \in \{1, \ldots, R\}$ follow a normal distribution with mean μ_{kr} and variance σ^2. μ_{kr} is chosen uniformly from a sequence $\{-10, -9, \ldots, 9, 10\}$. We vary the variance σ^2 to change the noise level, and the σ is chosen as $2, 4, 6, 8$, and 10 in our simulation settings, respectively. Both parameters ν_1, ν_2 for the bi-ADMM algorithm are set as 8.

We compare the performance of COBRA and bi-ADMM on identifying the bicluster structures in terms of the ARI. The mean values and the standard deviations of the ARI for each setting and algorithm across 100 replications are presented in Table 1. We can see that as σ increases, the ARIs for both COBRA and bi-ADMM methods decrease. These observations are reasonable because a larger σ implies a more challenging task to identify correct bicluster structures due to a higher level noise. In the meanwhile, given σ and M, a larger sample size implies better performance. For almost all settings, the bi-ADMM algorithm provide higher ARIs than those obtained by the COBRA. In particular, the superiority of bi-ADMM is substantial when the noise level is high. We note that the COBRA algorithm performs better in a single setting when $n = 200, p = 160, K = 16$, and $R = 8$, but the difference is not large. One possible reason is the unbalance between row

Table 1: Simulation results for the bi-ADMM and COBRA algorithms in terms of the ARI under various scenarios.

						bi-ADMM		COBRA	
n	p	K	R	M	σ	mean	sd	mean	sd
50	40	4	4	16	2	1.00	0.03	0.99	0.05
					4	0.96	0.09	0.88	0.15
					6	0.85	0.16	0.66	0.19
					8	0.65	0.21	0.42	0.17
		8	4	32	2	0.99	0.02	0.97	0.06
					4	0.92	0.08	0.82	0.12
					6	0.76	0.12	0.57	0.15
					8	0.54	0.16	0.33	0.12
100	80	4	4	16	2	1.00	0.00	1.00	0.02
					4	0.99	0.02	0.91	0.11
					6	0.86	0.15	0.54	0.16
					8	0.67	0.18	0.65	0.20
		8	4	32	4	0.98	0.04	0.92	0.11
					6	0.65	0.43	0.70	0.18
					8	0.53	0.12	0.53	0.14
		8	8	64	4	0.98	0.05	0.98	0.05
					6	0.83	0.17	0.81	0.13
					8	0.50	0.19	0.45	0.14
200	160	8	8	64	4	1.00	0.02	1.00	0.02
					6	0.93	0.06	0.96	0.05
					8	0.74	0.12	0.73	0.15
					10	0.46	0.14	0.39	0.13
		12	8	256	4	1.00	0.02	1.00	0.02
					6	0.98	0.03	0.96	0.05
					8	0.77	0.12	0.62	0.17
					10	0.40	0.15	0.28	0.10
		16	8	128	4	0.99	0.03	1.00	0.01
					6	0.88	0.07	0.94	0.06
					8	0.66	0.11	0.70	0.12
					10	0.44	0.12	0.36	0.11
		16	16	256	4	1.00	0.003	1.00	0.003
					6	0.98	0.03	0.96	0.05
					8	0.77	0.11	0.62	0.17
					10	0.40	0.15	0.28	0.10

and columns cluster sizes has negative impact on the performance of bi-ADMM, because n and p are close to each other.

4.2 Compositional Data

In this section, we evaluate the biclustering performance of biC-ADMM and COBRA algorithms using simulated compositional data based on a murine gut microbiome study (Livanos et al., 2016), which compared the gut microbiome between the group with early-life pulsed therapeutic antibiotic dosing (PAT) treatment and the group without any antibiotic treatment (control). In accordance with prior microbiome data analysis (Hu et al., 2018; Koh et al., 2017), we first generate OTU counts for 100 subjects from the Dirichlet-multinomial (DM) distribution, where the dispersion parameter and proportion means were estimated from the control microbiome samples of the murine study, and the total number of reads per sample is set to 10,000. As a demonstration, a subset of the OTU count data consisting of 36 mice and 24 common taxa with average proportation > 0.01 at age of 6 weeks is used in estimating the parameters of the DM distribution. Here the rule > 0.01 helps to remove the extremely rare taxa and to facilitate the following manipulation. Before we manually manipulate one half of the generated samples to create biclusters, using the original data we sort the average proportions of taxa in an ascending order and assign them into 3 groups: Group 1 has the first six taxa with the smallest proportions, accounting for 3% overall relative abundance on average; Group 2 has the last five taxa, accounting for 87% overall relative abundance on average; Group 3 has the remaining 13 taxa, accounting for 10% overall relative abundance on average. We manipulate the data in the following way. First, for each generated sample using the fitted DM model, we calculate the ratio of the summed counts for Group 2 over the summed counted for Group 1 (the averaged ratio is 126), and reduce the ratio by 1,400 folds. By doing that, we increased the relative abundance for taxa in Group 1 by roughly 93 folds from the original data. Second, we calculate the re-scaled counts for Groups 1 and 2 using the adjusted ratio by fixing the original total counts for Groups 1 and 2. Third, the count for each taxa in Groups 1 and 2 is re-scaled according to the ratio of the re-scaled group counts over the original

ones. Lastly, the relative abundance for this sample is obtained by standardizing it using the total counts. By doing these, the relative abundance of the taxa in Group 3 remains unchanged, denoted as "unchanged". Group 1 has its relative abundance enlarged for its taxa, while Group 2 has reduced relative abundance. Thus, Group 1 is denoted as "enlarged", and Group 2 is denoted as "shrunk". The 50 untouched samples are denoted as the "control" group, and the 50 manipulated samples are denoted as the "treatment" group. Then, the resulting data set has two row clusters and three column clusters.

Next, we evaluate the performance of COBRA and biC-ADMM algorithms on identifying the bicluster structure in terms of the ARI. The biculster structure with two row clusters and three column clusters may be artificial, so the ARI only serves as a reference metric. Under the compositional setting, a single tuning parameter γ for the COBRA is tuned, using the default setting provided by the R package "*cvxbiclustr*", and we adopt a two-dimensional grid search on γ_1 and γ_2 for the biC-ADMM method to allow for more flexibility.

Table 2 shows that the biC-ADMM is superior to the COBRA algorithm in terms of the ARI. For one simulated data set, the best tuning parameters are $\gamma_1 = 37.28$ and $\gamma_2 = 268.27$. Figure 2 presents the corresponding heat map based on the estimated $\widehat{\mathbf{A}}$. We can see that the biC-ADMM algorithm correctly identifies the "treatment" and "control" groups for samples. For column clusters, the taxa from the same groups are almost classified in the same algorithm-generated clusters. The five taxa in the group "shrunk" are included in two generated clusters with sizes as 1 and 4. The six taxa in the "enlarged" group are split into two clusters also, with one mixed into a cluster primarily formed by taxa from the "unchanged" group. Only one taxon from the "unchanged" group is merged with taxa from the "shrunk" group.

4.3 Computational Consideration

Step 2 in both Algorithms 1 and 2 involves solving the *Sylvester equation*, which imposes extra computational burden compared with the COBRA based on the DLPA. As we implement the up-to-date algorithm to solve such type of equation, it is interesting to compare the computational

Table 2: Simulations results for biC-ADMM and COBRA algorithms in terms of the ARI under the compositional setup.

biC-ADMM		COBRA	
mean	sd	mean	sd
0.54	0.10	0.48	0.09

Figure 2: Left panel: the heat map of the original simulated compositional data with 100 samples in 2 row clusters and 24 taxa in 3 column clusters. Right panel: the heat maps of $\widehat{\mathbf{A}}$ estimated by the biC-ADMM algorithm. The row(column) side color bars indicate the "true" row(column) clusters.

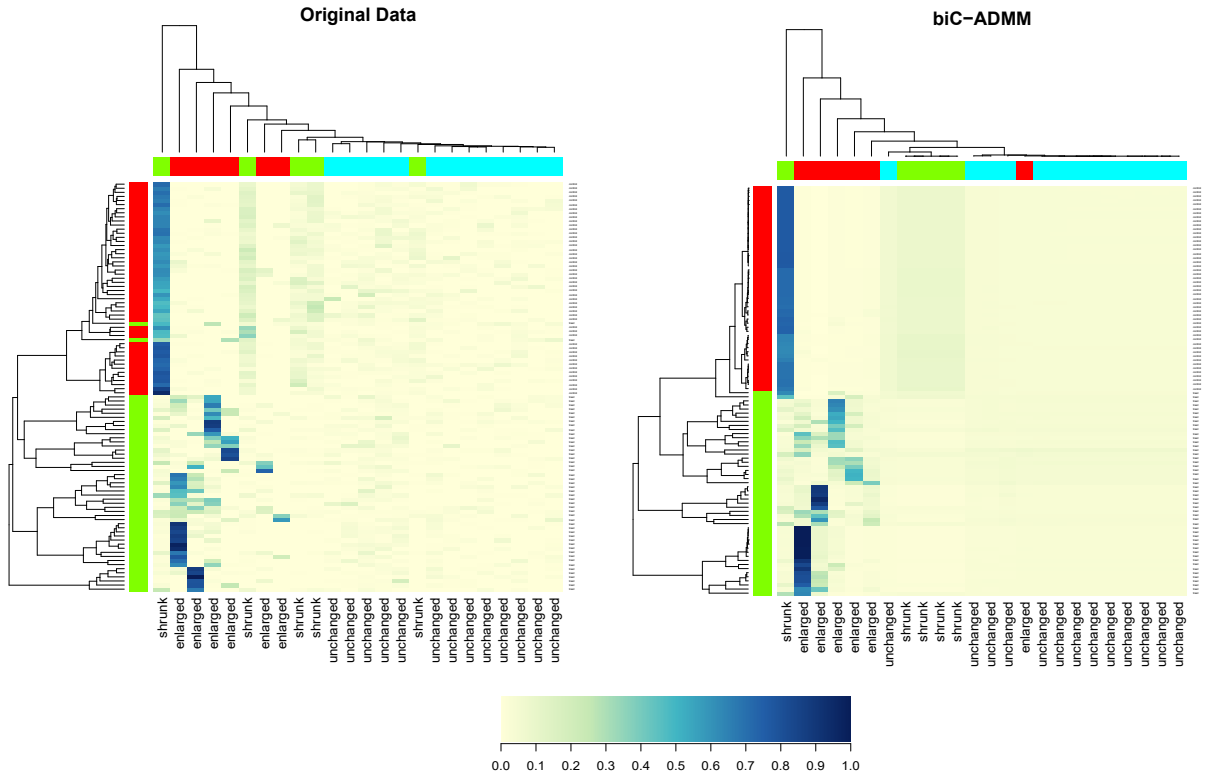

time of the proposed methods to the COBRA on various data settings. In this section, we evaluate the computational time in seconds of the COBRA and the bi-ADMM algorithm. The COBRA is implemented with the R package "*cvxbiclustr*" (Chi et al., 2017). We have developed an R package "*biADMM*" to implement our convex biclustering algorithms, bi-ADMM and biC-ADMM. To

improve the efficiency of the bi-ADMM algorithm, we also develop a Python version, which can be called back in R.

Table 3: Running time comparison with various combinations of n, p, K, R under the setting described in Section 4.1 with $\sigma = 2$ and a given tuning parameter $\gamma = 0.1$. The time is in seconds, which is an average across 30 replicates with 10 iterations for each algorithm.

	$n = 50$ $p = 40$ $K = 4$ $R = 4$	$n = 50$ $p = 40$ $K = 8$ $R = 4$	$n = 100$ $p = 80$ $K = 4$ $R = 4$	$n = 100$ $p = 80$ $K = 8$ $R = 4$	$n = 200$ $p = 160$ $K = 12$ $R = 8$	$n = 200$ $p = 160$ $K = 16$ $R = 8$
COBRA	0.001	0.001	0.008	0.014	0.046	0.038
bi-ADMM	0.791	0.788	7.786	7.765	104.208	104.386
bi-ADMM (Python)	0.072	0.075	0.657	0.617	6.247	6.336

The data sets are generated with the simulation settings described in Section 4.1. We set $\sigma = 2$ with a given tuning parameter $\gamma = 0.1$ defined in (10). Thirty replicates are simulated, and each algorithm is run for 10 iterations. Table 3 compares the average running time across 30 replicates of COBRA, bi-ADMM and Python-version bi-ADMM under various combinations of n, p, K and R. The COBRA shows its superiority in program efficiency, with the shortest running time and the slowest increase as the scenario gets more complicated. The Python-version bi-ADMM program improves the running time significantly compared with the R version. It is reasonable to pay acceptably more running time for better biclustering performance. The computer is equipped with a CPU i5-7267 (3.10 GHz) and 8G memory.

5 Application of biC-ADMM to a Gut Microbiome Data

Here, we apply the proposed biC-ADMM algorithm to the murine microbiome dataset used in simulation studies to assess the biclustering performance in compositional data. To be specific, we aim to simultaneously cluster a subset at 13 weeks with 37 common taxa and 68 samples, consisting of 32 microbiome samples from the PAT group and 36 control samples without retrieving their true

treatment group information. The left panel of Figure 3 shows the heat map and dendrogram of this data set. Since microbes in a community are usually dependent upon one another and may react similarly with environmental changes, it is of great interest to investigate whether there are multiple microbial taxa with the relative abundance being altered concordantly with the antibiotic treatment. In addition, the relative abundances of microbiome data are highly skewed, with a few common taxa accounting for the majority of bacteria in the sample. Microbiome studies usually need to group taxa at a higher rank to pull the signal strength. Some other research found that microbial community can be divided into sub-communities based on their functional reactions to the perturbation (Holmes et al., 2012; Sankaran and Holmes, 2019). All these observations motivate the application of clustering algorithm to identify data-driven taxa clusters co-expressed with the sample clusters.

Following the commonly used pre-processing step in microbiome data analysis, the OTU count data of each sample is normalized into relative abundances prior to conducting biclustering, i.e., with relative abundances of 37 taxa summing up to 1. In our biC-ADMM algorithm, we set $m_1 = m_2 = 5$ and $\phi = 0.5$ for weight w_l and u_k, and set $\nu_1 = \nu_2 = \nu_3 = 1$.

Then we apply the biC-ADMM algorithm to conduct convex biclustering for this data, which is an unsupervised learning method, free of a priori grouping knowledge. Although the true sample cluster labels are known, we mask them in biclustering analysis and aim to identify taxa clusters associated with potential sample subgroups. The tuning parameters are selected according to the stability selection in Section 3.2. The resulting optimal tuning parameters are $\gamma_1 = 297.64$ and $\gamma_2 = 29.76$.

First, we evaluate the performance of the biC-ADMM on identifying the known sample clusters. The estimate $\widehat{\mathbf{A}}$ provides two row clusters, and the confusion is shown in Table 4, indicating a misclassification rate of 13.2%, a sensitivity of 0.84, and a specificity of 0.89. Next, the resulting heat map is presented in the right panel of Figure 3, from which we can see four column clusters for the 37 taxa. The taxa "Akkermansia" and "Lactobacillus" are two individual clusters, which differ between the PAT and Control groups. The taxon "S24-7|Other" forms another cluster, with

Figure 3: Left panel: the heat map of the original microbiome data with 68 samples and 37 taxa. Right panel: the estimate $\widehat{\mathbf{A}}$ based on the biC-ADMM algorithm. The row(column) side color bars indicate the row(column) clusters based on the algorithms.

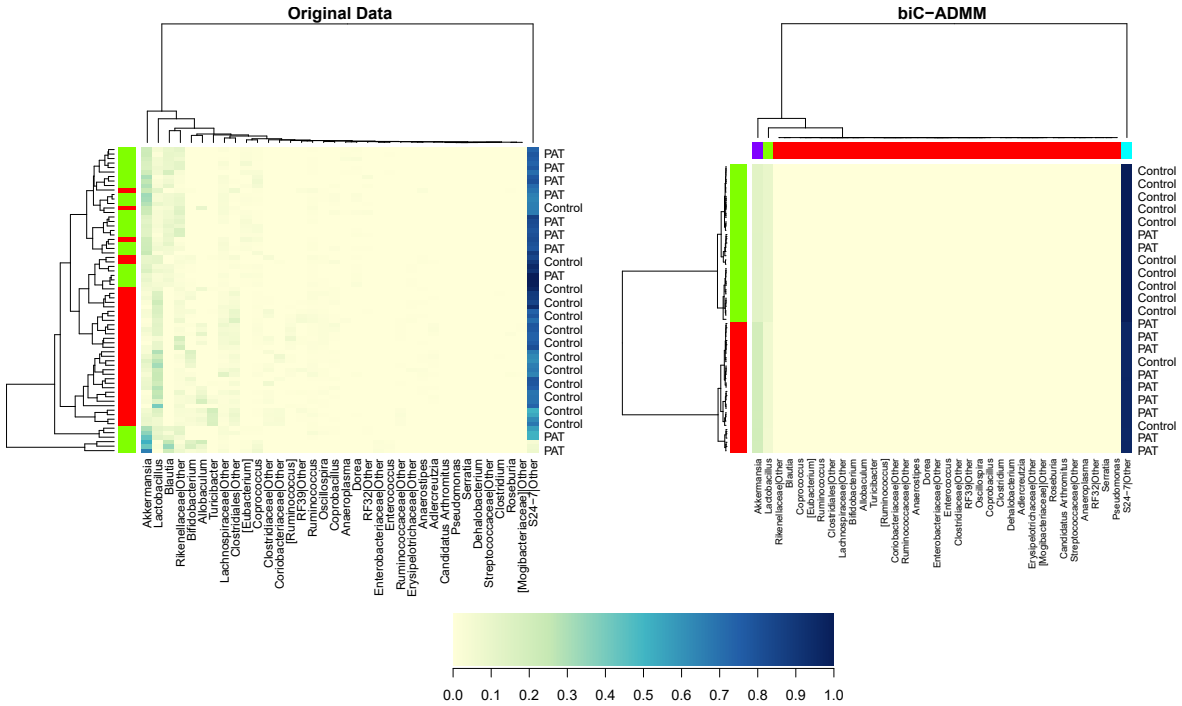

the largest relative abundance, but it does not differentiate the two groups. In order to confirm our findings, Wilcoxon's rank-sum test is used to compare the relative abundance of these three taxa between clusters generated by the biC-ADMM algorithm and between true cluster labels. Corresponding p-values are presented in Table 5. Those p-values are consistent with the biclusters identified by the biC-ADMM. The rest 34 taxa belong to the last cluster, which has a small relative abundance for both groups. Therefore, our algorithm provides a neat profile of these 37 taxa, which shows the PAT treatment changes the relative abundance of "Akkermansia" and "Lactobacillus" in the opposite direction.

Table 4: The confusion matrix for the sample (row) clusters based on biC-ADMM algorithm.

	Reference	
Prediction	Control	PAT
Control	32	5
PAT	4	27

Table 5: P-values for the comparisons of the selected genuses between row clusters, using Wilcoxon's rank-sum test.

	"Akkermansia"	"Lactobacillus"	"S24-7|Other"
Row clusters based on the biC-ADMM	4.0e-15	5.1e-9	0.17
True row clusters	7.0e-12	1.0e-10	0.66

6 Summary

Biclustering is a powerful data mining technique which can provide results in a checkerboard-like pattern to explore the co-expressed features for subgroups, while it is under-utilized in biological and biomedical data. Among biclustering algorithms developed in the past two decades, the convex biclustering algorithm is appealing due to its globally optimal solution. However, existing convex biclustering solved the convex optimization problem via an approximation to objective function of the ADMM algorithm, which required extra smoothing steps to obtain informative biclusters. On the other hand, existing biclustering methods cannot incorporate the compositional constraints which are often needed for the increasingly popular microbiome data.

In this manuscript, a new algorithm for the standard convex biclustering and its extension under the compositional constraints are proposed to simultaneously cluster observations and features, denoted as the bi-ADMM and the biC-ADMM, respectively. Both algorithms directly apply the ADMM method with solving a *Sylvester Equation* as a key step, which has a great potential to solve other problems with both row and columns constraints for a data matrix. The numerical results show that bi-ADMM and biC-ADMM are able to provide clear checker-board like pattern directly without any further smoothing step. Furthermore, the biC-ADMM can solve biclustering problems with compositional constraints, and it can be extended to any linear constraint easily, which has a great potential to be used in microbiome studies. Furthermore, we have developed an R package "*biADMM*" to implement our convex biclustering algorithms, bi-ADMM and biC-ADMM, which includes Python-version functions to speed up the calculation.

Moreover, this work can motivate future research. Wang et al. (2018) presented the *Sparse Convex Clustering* problem, seeking to cluster observations and select features simultaneously. Feature

selection can be incorporated into the convex biclustering as well. In addition, Zhou et al. (2020) developed a very efficient smoothing proximal gradient algorithm (Sproga) for convex clustering. Then, we can extend convex biclustering to sparse convex biclustering and develop a highly efficient algorithms to solve it, in order to conduct biclustering and feature selection simultaneously. Furthermore, weights w_l and u_k serves important roles in convex biclustering, but they suffer from the variable selection problem (Chakraborty and Xu, 2020). The proposed algorithms can be improved in this direction as well.

Acknowledgement

Hu and Li's research is partially supported by a National Institute of Health (NIH) grant (5R01DK110014).

References

Busygin, S., Prokopyev, O., and Pardalos, P. M. (2008). Biclustering in data mining. *Computers & Operations Research*, 35(9):2964–2987.

Chakraborty, S. and Xu, J. (2020). Biconvex clustering.

Cheng, Y. and Church, G. M. (2000). Biclustering of expression data. In *Ismb*, volume 8, pages 93–103.

Chi, E. C., Allen, G. I., and Baraniuk, R. G. (2017). Convex biclustering. *Biometrics*, 73(1):10–19.

Chi, E. C. and Lange, K. (2015). Splitting Methods for Convex Clustering. *Journal of Computational and Graphical Statistics*, 24(4):994–1013.

Falony, G., Joossens, M., Vieira-Silva, S., Wang, J., Darzi, Y., Faust, K., Kurilshikov, A., Bonder, M. J., Valles-Colomer, M., Vandeputte, D., et al. (2016). Population-level analysis of gut microbiome variation. *Science*, 352(6285):560–564.

Fang, Y. and Wang, J. (2012). Selection of the number of clusters via the bootstrap method. *Computational Statistics & Data Analysis*, 56:468–477.

Friedman, J., Hastie, T., and Tibshirani, R. (2001). *The elements of statistical learning*, volume 1. Springer series in statistics New York.

Gloor, G. B., Macklaim, J. M., Pawlowsky-Glahn, V., and Egozcue, J. J. (2017). Microbiome datasets are compositional: and this is not optional. *Frontiers in microbiology*, 8:2224.

Hochreiter, S., Bodenhofer, U., Heusel, M., Mayr, A., Mitterecker, A., Kasim, A., Khamiakova, T., Van Sanden, S., Lin, D., Talloen, W., et al. (2010). Fabia: factor analysis for bicluster acquisition. *Bioinformatics*, 26(12):1520–1527.

Holmes, I., Harris, K., and Quince, C. (2012). Dirichlet multinomial mixtures: generative models for microbial metagenomics. *PloS one*, 7(2):e30126.

Hripcsak, G. and Albers, D. J. (2012). Next-generation phenotyping of electronic health records. *Journal of the American Medical Informatics Association*, 20(1):117–121.

Hu, J., Koh, H., He, L., Liu, M., Blaser, M. J., and Li, H. (2018). A two-stage microbial association mapping framework with advanced fdr control. *Microbiome*, 6(1):131.

Hubert, L. and Arabie, P. (1985). Comparing partitions. *Journal of classification*, 2(1):193–218.

Jameson, A. (1968). Solution of the equation ax+xb=c by inversion of an m*m or n*n matrix. *SIAM Journal on Applied Mathematics*, 16(5):1020–1023.

Koh, H., Blaser, M. J., and Li, H. (2017). A powerful microbiome-based association test and a microbial taxa discovery framework for comprehensive association mapping. *Microbiome*, 5(1):45.

Livanos, A. E., Greiner, T. U., Vangay, P., Pathmasiri, W., Stewart, D., McRitchie, S., Li, H., Chung, J., Sohn, J., Kim, S., et al. (2016). Antibiotic-mediated gut microbiome perturbation accelerates development of type 1 diabetes in mice. *Nature microbiology*, 1(11):1–13.

Madeira, S. C. and Oliveira, A. L. (2004). Biclustering algorithms for biological data analysis: a survey. *IEEE/ACM Transactions on Computational Biology and Bioinformatics (TCBB)*, 1(1):24–45.

Sankaran, K. and Holmes, S. P. (2019). Latent variable modeling for the microbiome. *Biostatistics*, 20(4):599–614.

Sorensen, D. C., Zhou, Y., et al. (2003). Direct methods for matrix sylvester and lyapunov equations. *Journal of Applied Mathematics*, 6(2003):277–303.

Tibshirani, R., Saunders, M., Rosset, S., Zhu, J., and Knight, K. (2005). Sparsity and smoothness via the fused lasso. *Journal of the Royal Statistical Society: Series B*, 67:1198–1232.

Wang, B., Zhang, Y., Sun, W. W., and Fang, Y. (2018). Sparse convex clustering. *Journal of Computational and Graphical Statistics*, 27:393–403.

Xie, J., Ma, A., Fennell, A., Ma, Q., and Zhao, J. (2018). It is time to apply biclustering: a comprehensive review of biclustering applications in biological and biomedical data. *Briefings in bioinformatics*, 1:16.

Zhou, X., Du, C., and Cai, X. (2020). An efficient smoothing proximal gradient algorithm for convex clustering. *arXiv preprint arXiv:2006.12592*.

Appendix

In Appendix, we provide proofs of Lemma 1 and Lemma 2.

Proof of Lemma 1

Denote $\mathbf{a} = \text{vec}(\mathbf{A})$, a vectorization of the matrix $\mathbf{A}$. According to the fact that $A_{i_1\cdot} - A_{i_2\cdot} = \mathbf{A}^{\mathrm{T}}(\mathbf{e}_{i_1} - \mathbf{e}_{i_2})$, $\mathbf{a}_{k_1} - \mathbf{a}_{k_2} = \mathbf{A}(\mathbf{e}^*_{k_1} - \mathbf{e}^*_{k2})$, and the property of the tensor product $\text{vec}(\mathbf{RST}) =$

$[\mathbf{T}^{\mathrm{T}} \otimes \mathbf{R}]\mathrm{vec}(\mathbf{S})$, solving the minimization of $f(\mathbf{A})$ is equivalent to minimize

$$f(\mathbf{a}) = \frac{1}{2}\|\mathbf{x} - \mathbf{a}\|_2^2 + \frac{\nu_1}{2}\sum_{l \in \mathcal{E}_l} \|\mathbf{B}_l \mathbf{P}\mathbf{a} - \widetilde{\mathbf{v}}_l\|_2^2 + \frac{\nu_2}{2}\sum_{k \in \mathcal{E}_2} \|\mathbf{C}_k \mathbf{a} - \widetilde{\mathbf{z}}_k\|_2^2,$$

where $\mathbf{B}_l, \mathbf{C}_k$ and $\mathbf{P}$ are defined in Section 2.3. Then it follows that

$$f(\mathbf{a}) = \frac{1}{2}\|\mathbf{x} - \mathbf{a}\|_2^2 + \frac{\nu_1}{2}\|\mathbf{B}\mathbf{P}\mathbf{a} - \widetilde{\mathbf{v}}\|_2^2 + \frac{\nu_2}{2}\|\mathbf{C}\mathbf{a} - \widetilde{\mathbf{z}}\|_2^2,$$

where $\mathbf{B}, \mathbf{C}, \widetilde{\mathbf{v}}$ and $\widetilde{\mathbf{z}}$ are defined in Section 2.3 as well.

Finally, the stationary equation can be obtained by

$$(\mathbf{I}_{np} + \nu_1 \mathbf{P}^{\mathrm{T}}\mathbf{B}^{\mathrm{T}}\mathbf{B}\mathbf{P} + \nu_2 \mathbf{C}^{\mathrm{T}}\mathbf{C})\mathbf{a} = \mathbf{x} + \nu_1 \mathbf{P}^{\mathrm{T}}\mathbf{B}^{\mathrm{T}}\widetilde{\mathbf{v}} + \nu_2 \mathbf{C}^{\mathrm{T}}\widetilde{\mathbf{z}}.$$

This is a system of np linear equations. By applying the properties for Kronecker product such as $(\mathbf{S} \otimes \mathbf{T})^{\mathrm{T}} = \mathbf{S}^{\mathrm{T}} \otimes \mathbf{T}^{\mathrm{T}}$ and $(\mathbf{Q} \otimes \mathbf{R})(\mathbf{S} \otimes \mathbf{T}) = (\mathbf{Q}\mathbf{S}) \otimes (\mathbf{R}\mathbf{T})$, it follows

$$\begin{aligned}
\nu_2 \mathbf{C}^{\mathrm{T}}\mathbf{C} &= \nu_2 \sum_{k \in \mathcal{E}_2} \left[\left((\mathbf{e}_{k_1}^* - \mathbf{e}_{k_2}^*)(\mathbf{e}_{k_1}^* - \mathbf{e}_{k_2}^*)^{\mathrm{T}}\right)\right] \otimes \mathbf{I}_n \\
&= \left[\sum_{k \in \mathcal{E}_2} \nu_2 \left((\mathbf{e}_{k_1}^* - \mathbf{e}_{k_2}^*)(\mathbf{e}_{k_1}^* - \mathbf{e}_{k_2}^*)^{\mathrm{T}}\right)\right] \otimes \mathbf{I}_n \\
\nu_2 \mathbf{C}^{\mathrm{T}}\widetilde{\mathbf{z}} &= \nu_2 \sum_{k \in \mathcal{E}_2} [(\mathbf{e}_{k_1}^* - \mathbf{e}_{k_2}^*) \otimes \mathbf{I}_n]\widetilde{\mathbf{z}}_k \\
&= \sum_{k \in \mathcal{E}_2} \left(\nu_2 (\mathbf{e}_{k_1}^* - \mathbf{e}_{k_2}^*) \otimes \mathbf{I}_n\right) \widetilde{\mathbf{z}}_k \\
\nu_3 \mathbf{D}^{\mathrm{T}}\mathbf{D} &= \nu_3 \sum_{i=1}^{n} \mathbf{D}_i^{\mathrm{T}}\mathbf{D}_i = \nu_3 (\mathbf{1}_p \mathbf{1}_p^{\mathrm{T}}) \otimes \mathbf{I}_n \\
\nu_3 \mathbf{D}^{\mathrm{T}}\mathbf{s} &= \nu_3 \sum_{i=1}^{n} (\mathbf{1}_p \otimes \mathbf{e}_i) s_i = \nu_3 \sum_{i=1}^{n} s_i \mathrm{vec}(\mathbf{e}_i \mathbf{1}_p^{\mathrm{T}}).
\end{aligned}$$

In addition, by applying Proposition 1 in Wang et al. (2018) for the permutation matrix $\mathbf{P}$, we

can prove

$$\begin{aligned}\mathbf{I}_{np} + \nu_1 \mathbf{P}^{\mathrm{T}}\mathbf{B}^{\mathrm{T}}\mathbf{B}\mathbf{P} &= \mathbf{I}_p \otimes \left[\mathbf{I}_n + \nu_1 \sum_{l\in\mathcal{E}_1} (\mathbf{e}_{l_1} - \mathbf{e}_{l_2})(\mathbf{e}_{l_1} - \mathbf{e}_{l_2})^{\mathrm{T}}\right] \\ \nu_1 \mathbf{P}^{\mathrm{T}}\mathbf{B}^{\mathrm{T}}\widetilde{\mathbf{v}} &= \sum_{l\in\mathcal{E}_1} \left(\mathbf{I}_p \otimes \nu_1(\mathbf{e}_{l_1} - \mathbf{e}_{l_2})\right)\widetilde{\mathbf{v}}_l.\end{aligned}$$

Therefore, the system of equations is equivalent to

$$(\mathbf{I}_p \otimes \mathbf{M})\mathrm{vec}(\mathbf{A}) + (\mathbf{N} \otimes \mathbf{I}_n)\mathrm{vec}(\mathbf{A}) = \mathrm{vec}(\mathbf{G}),$$

which is equivalent to $\mathbf{M}\mathbf{A} + \mathbf{A}\mathbf{N} = \mathbf{G}$. □

Proof of Lemma 2

Proof of Lemma 1 needs to be modified to incorporate the extra constraints. The stationary equations for minimizing (8) can be obtained by

$$(\mathbf{I}_{np} + \nu_1 \mathbf{P}^{\mathrm{T}}\mathbf{B}^{\mathrm{T}}\mathbf{B}\mathbf{P} + \nu_2 \mathbf{C}^{\mathrm{T}}\mathbf{C} + \nu_3 \mathbf{D}^{\mathrm{T}}\mathbf{D})\mathbf{a} = \mathbf{x} + \nu_1 \mathbf{P}^{\mathrm{T}}\mathbf{B}^{\mathrm{T}}\widetilde{\mathbf{v}} + \nu_2 \mathbf{C}^{\mathrm{T}}\widetilde{\mathbf{z}} + \nu_3 \mathbf{D}^{\mathrm{T}}\mathbf{s}.$$

With matrix techniques, it follows

$$\begin{aligned}\nu_3 \mathbf{D}^{\mathrm{T}}\mathbf{D} &= \nu_3 \sum_{i=1}^{n} \mathbf{D}_i^{\mathrm{T}}\mathbf{D}_i = \nu_3(\mathbf{1}_p\mathbf{1}_p^{\mathrm{T}}) \otimes \mathbf{I}_n \\ \nu_3 \mathbf{D}^{\mathrm{T}}\mathbf{s} &= \nu_3 \sum_{i=1}^{n} (\mathbf{1}_p \otimes \mathbf{e}_i)s_i = \nu_3 \sum_{i=1}^{n} s_i \mathrm{vec}(\mathbf{e}_i\mathbf{1}_p^{\mathrm{T}}).\end{aligned}$$

Therefore, the system of equations is equivalent to

$$(\mathbf{I}_p \otimes \mathbf{M})\mathrm{vec}(\mathbf{A}) + (\mathbf{N} \otimes \mathbf{I}_n)\mathrm{vec}(\mathbf{A}) = \mathrm{vec}(\mathbf{G}).$$

□